1 Introduction

1.1 Optical pulses and their applications

Light pulses are always intriguing as they interact with the medium for a short time duration and exhibits various exclusive temporal as well as spectral domain phenomena. One can efficiently generate such optical pulses through lasers with their duration of existence, namely *pulse width*, ranging from nanoseconds (10^{-9} s) to femtoseconds (10^{-15} s). Q-switched lasers emit light pulses in nanosecond duration with sufficiently high energies (in milliJoule or higher), whereas mode-locked lasers emit low energy ultrashort optical pulses. Moreover, such light pulses are commercially available in certain temporal shapes (the optical power distribution profile with time) such as Gaussian, hyperbolic secant, super-Gaussian etc. Depending on pulse's temporal shape, their width and energy content become different and must be accounted separately. Besides, pulse spectral profile and phase are also important and their uses are often application specific. This thesis aims to study the dynamics of such ultrashort optical pulses in linear, nonlinear and time-varying media for targeted specialty applications.

1.1.1 Ultrashort optical pulses and their utilities

Light pulses with their widths ranging from picoseconds (10^{-12} s) to femtoseconds (10^{-15} s) are known as *ultrashort optical pulses*. Such pulses have wide optical spectra and can be efficiently generated from fiber lasers, semiconductor lasers etc. with mode-locked operation [Shank, 1988]. Such optical pulses usually contain low energy, in nano-Joule (nJ) or pico-Joule (pJ) range, however they can have a high peak power and in turn a high intensity owing to their short pulse width. Such high power ultrashort pulses are readily used for triggering various nonlinear phenomena through light-matter interaction. As an example, generation of supercontinuum, second harmonic generation etc. are done using femtosecond pulses where the peak power may reach killoWatt (kW) range. Their short temporal widths are much suitable for time-resolved measurements of ultrafast phenomena, whereas the corresponding wide spectral bandwidth can eventually be used for various spectroscopic investigations [Kobayashi, 2018; Luo et al., 2022]. A high power ultrashort pulse is very much suitable for certain industrial processes like micromachining, remote sensing etc [Samad et al., 2012]. Such high power pulses are also applicable to noninvasive bio-medical surgery, tissue or tumor ablation, skin rejuvenation and many more [Marble and Yakovlev, 2020; Conkey et al., 2017]. Lately, high power ultrashort pulsed lasers are being used for strategic purposes like laser detonators etc [Kennedy, 2006]. Moreover, the existing ultrafast optical network for data transmission utilizes such short pulse widths with a relatively low power scale to avoid nonlinear interactions and smooth transfer of information [Keeler et al., 2003].

All of these utilities of ultrashort optical pulses eventually require distortion free pulse dynamics during their transmission through the medium. It is important to mention here that the stability of such ultrashort pulses inside a medium depends on three major physical factors, namely *loss*, *dispersion*, and *nonlinearity*, which if unaccounted may have harsh impact on pulse propaga-

tion dynamics, thereby leading to pulse distortion and massive failure of the targeted application. Moreover, these three prime factors are associated with the material properties as well as the structural properties of the medium. In this thesis, two separate classes of medium has been considered to study the dynamics of ultrashort optical pulses and their stable delivery through them. As a static system, optical fiber has been considered which is a micrometer-thick cylindrical dielectric waveguide with a spatially varying refractive index profile. It is to mention here that the fibers are widely known for their structural flexibility and integration compatibility with the existing infrastructure that eventually opens up a myriad of applications. Moreover, they are the only waveguide that support robust guided delivery of light over short as well as long distances. On the other hand, a linear bulk medium that exclusively contains a temporally varying refractive index profile has been considered as the dynamic system that has high potential to exhibit unique states of light. In the next section, the three limiting factors of ultrashort pulse propagation and their impacts on pulse dynamics during propagation through optical fibers will be discussed.

1.2 Propagation of optical pulses in optical fibers

A typical optical fiber is a cylindrical dielectric waveguide with spatial inhomogeneity that creates a central transparent region for light propagation known as "fiber core" surrounded by a region known as cladding. When an electromagnetic (EM) wave enters an optical fiber, it appears to form certain field distributions for a given optical frequency and polarization in a plane perpendicular to the propagation direction. However, only few field distributions within the core region do not change during their propagation except a phase change, and are associated with the well-known fiber modes. Also, each mode is associated with a propagation constant β which is a function of optical frequency ω. Moreover, an all-solid dielectric fiber comprises of materials such as glass, plastics, ceramics etc. An optical pulse propagates through the fiber being associated with a particular fiber mode. Thus, the propagating pulse acquires all of the modal characteristics such as dispersion, loss, and nonlinearity associated with that particular mode and exhibits specific propagation dynamics.

1.2.1 Effect of dispersion

Dispersion is a phenomenon that causes temporal width of the pulse to be broadened during propagation. In optical fibers, there are two components of the total dispersion, namely material dispersion, and waveguide dispersion. The material contribution to the dispersion occurs through the frequency dependence of the refractive index $n(\omega)$ of the medium that arises from the interaction of EM wave and bound electrons of dielectric materials. It is well-known as chromatic dispersion whose origin is related to the characteristic resonance frequencies of the material at which the EM waves get absorbed via oscillations of bound electrons. In optical fibers, it is well-approximated far from the medium resonances by the empirical formula [Agrawal, 2019a],

$$n^2(\omega) = 1 + \frac{B_1\omega_1^2}{\omega_1^2 - \omega^2} + \frac{B_2\omega_2^2}{\omega_2^2 - \omega^2} + \frac{B_3\omega_3^2}{\omega_3^2 - \omega^2} \tag{1.1}$$

where, ω_j are the resonance frequencies, and B_j are the strength of the corresponding resonances with $j = 1, 2, 3$, which are to be determined experimentally. Equation 1.1 can also be written in terms of wavelength λ as,

$$n^2(\lambda) = 1 + \frac{B_1\lambda^2}{\lambda^2 - \lambda_1^2} + \frac{B_2\lambda^2}{\lambda^2 - \lambda_2^2} + \frac{B_3\lambda^2}{\lambda^2 - \lambda_3^2} \tag{1.2}$$

where, $\lambda_j = \omega_j/2\pi c$ with c being the speed of light in vacuum.

The contribution to the dispersion introduced through the fiber cross-section and mode profile is termed as waveguide dispersion. This occurs from the fact that during propagation, light spreads into the cladding region from the core region where there exist an index difference between the two, and that leads to a change in the mode field diameter (MFD) as a function of frequency/wavelength. Eventually, frequency dependence of MFD introduces a change in velocity which is also frequency dependent, thereby leading to waveguide dispersion. MFD is usually different than the geometric core diameter. Considering the mode-field distribution to be Gaussian, MFD can be obtained by the relation,

$$\text{MFD} = 2\sqrt{\frac{A_{eff}}{\pi}} \tag{1.3}$$

where, A_{eff} is termed as the effective mode area defined as,

$$A_{eff} = \frac{(\int\int_{-\infty}^{\infty} |F(x,y)|^2 dxdy)^2}{\int\int_{-\infty}^{\infty} |F(x,y)|^4 dxdy}. \tag{1.4}$$

where $F(x,y)$ is the modal distribution of the EM wave inside the fiber. The total dispersion is introduced in pulse propagation through the propagation constant $\beta(\omega) = n(\omega)\omega/c$ associated with the fiber modes, where $n(\omega)$ is the effective refractive index considering both the material and waveguide contribution.

To understand the origin of dispersion-induced pulse broadening, let us consider the optical pulse as an electromagnetic envelope with a finite number of frequency components included within the spectrum of width $\Delta\omega$. Inside the fiber, The various spectral components of the pulse experience different speed owing to the relation $v = c/n(\omega)$, and travel with different phase velocities defined as

$$v_p = \omega/\beta, \tag{1.5}$$

where $\beta = nk$ is the propagation constant of the wave with $k = 2\pi/\lambda = \omega/c$ known as the wave number. However, the envelope of the pulse propagates through the medium with a velocity slightly different from all the phase velocities, and is called group velocity v_g defined as,

$$v_g = \frac{d\omega}{d\beta}. \tag{1.6}$$

which remains nearly a constant for optical pulses with narrow spectral width where the spectral components have nearly equal frequencies. However, situation becomes complex for ultrashort pulses, where their relatively broad spectrum causes the group velocity v_g to be dependent on frequency ω that ultimately leads to the dispersion of group velocity, termed as *group velocity dispersion* (GVD). In that case, due to traveling with different speeds, the various pulse parts reach the output end at different times. As a result, the pulse gets broadened in time domain as shown in figure 1.1. The phenomenon of dispersion in fibers can be understood mathematically by considering the frequency dependent propagation constant $\beta(\omega)$ associated with the fiber mode given as,

$$\beta(\omega) = \frac{n(\omega)\omega}{c} = \beta_0 + \beta_1(\omega - \omega_0) + \frac{1}{2}\beta_2(\omega - \omega_0)^2 + \cdots \tag{1.7}$$

where it has been expanded in a Taylor series around the central pulse frequency ω_0 under an approximation that the finite width of the pulse spectrum is much less than the central frequency i.e., $\Delta\omega/\omega_0 << 1$. In equation (1.7), the various coefficients are defined as,

$$\beta_m = \left.\frac{d^m\beta}{d\omega^m}\right|_{\omega=\omega_0} \qquad \text{with} \qquad m = 0, 1, 2, ... \tag{1.8}$$

from which the physical meaning of parameters β_1 and β_2 can be explicitly explained. By taking the first order derivative of $\beta(\omega)$, one obtains the relation,

$$\beta_1 = \frac{1}{c}\left(n + \frac{dn}{d\omega}\right) = \frac{n_g}{c} = \frac{1}{v_g}, \tag{1.9}$$

where n_g is the group index of the pulse. Equation (1.9) readily dictates that the coefficient β_1 is the inverse of the group velocity with which the pulse travels inside the fiber. Similarly, the second order derivative of $\beta(\omega)$ gives the expression,

$$\beta_2 = \frac{1}{c}\left(2\frac{dn}{d\omega} + \omega\frac{d^2n}{d\omega^2}\right), \tag{1.10}$$

which represents the dispersion of group velocity, widely known as GVD parameter, and is responsible for the pulse broadening. Depending on the sign of GVD parameter β_2, there are two types of dispersion regime - anomalous dispersion when $\beta_2 < 0$, and normal dispersion when $\beta_2 > 0$. Also, a wavelength dependent dispersion quantity D can also be defined as,

$$D = \frac{d\beta_1}{d\lambda} = -\frac{2\pi c}{\lambda^2}\beta_2 = -\frac{\lambda}{c}\frac{d^2n}{d\lambda^2}. \tag{1.11}$$

This quantity is termed as the dispersion parameter and can directly be estimated if the effective index of the mode is known. Moreover, the length scale over which the effect of dispersion becomes important is referred to as dispersion length, and is denoted by,

$$L_D = \frac{T_0^2}{|\beta_2|}, \tag{1.12}$$

where T_0 is pulse width.

Such dispersion-induced temporal broadening becomes detrimental for applications where data transmission occurs through short optical pulses. There is a huge possibility that temporally broadened pulses will overlap with each other which leads to pulse distortion and loss of information. Besides GVD, there are higher order dispersion present in a fiber that too causes pulse distortion. Specifically, the third order dispersion introduced through the coefficient β_3 in equation (1.7) becomes significant during pulse propagation around a nearly zero GVD. Since the effect of dispersion is unavoidable during ultrashort pulse propagation, it is mandatory to manage the total fiber dispersion with some judicious arrangement, either in terms of input pulse parameter customization or in terms of waveguide engineering.

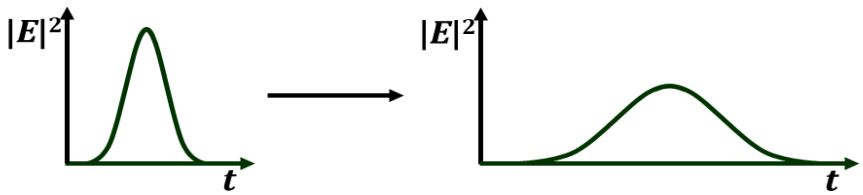

Figure 1.1: The schematic representation of dispersion-induced pulse broadening during propagation in a dielectric waveguide.

1.2.2 Effect of nonlinearity

Nonlinearity in optical fibers arises from the nonlinear interaction of a high intensity EM wave and the bound electrons of the dielectric. An ultrashort pulse associated with a high intensity

eventually triggers nonlinear interactions. The higher order susceptibilities present in the induced field polarization gives rise to various nonlinear optical phenomena along with the basic linear contributions. To begin with, it is important to establish the relation between the the total induced polarization $\mathbf{P}$ and the electric field $\mathbf{E}$ inside the fiber. In that case, the total polarization $\mathbf{P}$, away from the resonance of the medium, is written in a more general form as [Agrawal, 2019a],

$$\mathbf{P} = \epsilon_0 \left(\chi^{(1)} \cdot \mathbf{E} + \chi^{(2)} : \mathbf{EE} + \chi^{(3)} \vdots \mathbf{EEE} + \cdots \right) \tag{1.13}$$

where, $\chi^{(j)}$ is the susceptibility of jth order. The first order susceptibility $\chi^{(1)}$ is the linear dominant contribution to $\mathbf{P}$ which is generally a complex quantity. The inclusion of the effect of $\chi^{(1)}$ occurs through the refractive index $n(\omega)$ and attenuation constant $\alpha(\omega)$. The second term containing $\chi^{(2)}$ in the R.H.S of equation (1.13) provides a nonlinear contribution and becomes important only when there is an asymmetry in the molecular level of the material which is generally rare for optical fibers. It eventually leads to nonlinear phenomena like second harmonic generation. The most common and the lowest order nonlinear contribution in fibers comes from the third order susceptibility term $\chi^{(3)}$ which gives rise to effects like nonlinear refraction, third harmonic generation, four wave mixing etc. However, the nonlinear refraction is the most basic nonlinear process that do not require any prior phase-matching condition to satisfy; rather it occurs through a nonlinear phase shift due to an instantaneous response of the bound electrons exhibiting intensity-dependent refractive index, termed as Kerr effect. In this case, the refractive index is a function of both the frequency ω and the intensity I of light, and is written as,

$$\tilde{n}(\omega, I) = n(\omega) + n_2 I = n + \bar{n}_2 |E|^2, \tag{1.14}$$

where, I is the light intensity and related to the wave amplitude as $I = |E|^2$; $\bar{n}_2$ is the nonlinear-index coefficient and is related to the real part of the third order susceptibility term as,

$$\bar{n}_2 = \frac{3}{8n} \mathrm{Re}(\chi^{(3)}_{xxxx}) \tag{1.15}$$

where, the electric field E is assumed to be linearly polarized so that only one component of the susceptibility tensor contributes to the refractive index. Moreover, $\bar{n}_2$ is a material specific parameter which is directly related to the nonlinear coefficient γ through the relation [Agrawal, 2019b],

$$\gamma(\omega_0) = \frac{\omega_0 \bar{n}_2 \iint_{-\infty}^{\infty} |F(x,y)|^4 dxdy}{c \iint_{-\infty}^{\infty} |F(x,y)|^2 dxdy}, \tag{1.16}$$

where, ω_0 is the pulse central frequency, c the speed of light in vacuum, and $F(x, y)$ is the modal distribution of the EM wave inside the fiber. The expression for $\gamma(\omega_0)$ can be redefined as,

$$\gamma(\omega_0) = \frac{\omega_0 n_2}{c A_{eff}}, \tag{1.17}$$

where, $n_2 = 2\bar{n}_2/\epsilon_0 nc$ is called Kerr coefficient having a unit of m^2/W, and A_{eff} is given in equation (1.4). Thus, γ is expressed in units of $\mathrm{W}^{-1}/\mathrm{m}$. The estimation of γ using equation (1.17) clearly requires the knowledge of the modal field distribution that in turn depends on the two fiber parameters such as core radius and core-clad index difference. A_{eff} has a significant role to play in the occurrence of nonlinearity which is controlled entirely by the fiber design specifications. Hence, it is explicit that the effect of nonlinearity can be reduced or enhanced by varying the effective mode area. The coefficient γ is responsible for two basic nonlinear phenomena - self-phase modulation (SPM) and cross-phase modulation (XPM) which essentially introduces spectral broadening of ultrashort pulses. SPM is the most common nonlinear effect induced via Kerr nonlinearity during pulse propagation, whereas XPM comes into play for co-propagating optical pulses. In SPM, an

ultrashort pulse experiences a self-induced nonlinear phase shift during its propagation through a fiber of length L that can be obtained by noting the phase of the field change,

$$\phi = (n + \bar{n}_2|E|^2)k_0 L \tag{1.18}$$

where, $k_0 = 2\pi/\lambda$. In this process, new frequency components are generated owing to the nonlinear phase shift $\phi_{NL} = \bar{n}_2|E|^2 k_0 L$ which broadens the pulse spectrum as shown in figure 1.2. However, excessive nonlinear phase accumulation induced by very high pulse intensity destroy the pulse both in spectral and in temporal domain. The fiber length over which the effect of nonlinearity becomes important is referred to as nonlinear length, and is given by,

$$L_{NL} = \frac{1}{\gamma P_0}, \tag{1.19}$$

where, P_0 is the pulse peak-power.

Beside SPM, intrapulse Raman scattering (IRS) is the common higher order nonlinear effect induced through the delayed response of the nuclei of the medium, and should be included during the propagation of input pulses with spectral width $>$ 0.1THz. In presence of IRS, a red shift (energy transfer from high frequency component to low frequency component) in the pulse spectrum occurs during its propagation due to Raman gain, and is referred as Raman-induced frequency shift. Moreover, self-steepening (SS), and two-photon absorption (TPA) are few important higher order nonlinear effects that should be taken into account for very high peak power or pulse widths $<$ 100 fs. Such nonlinearities essentially perturb the stable propagation of pulses leading to unwanted phenomena like asymmetric pulse shape, optical shock, nonlinear absorption etc. during the pulse evolution. In this context, SPM-induced nonlinear effects can be beneficial only in presence of GVD if the respective phase contributions are made to balance or cancel each other by some technique. In this case, one may observe exclusive pulse dynamics such as optical solitons and similaritons.

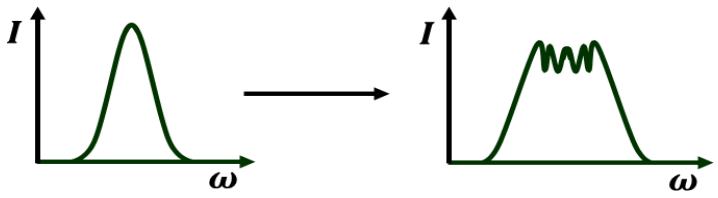

Figure 1.2: The schematic representation of nonlinearity-induced spectral broadening during propagation in a dielectric waveguide.

1.2.3 Effect of loss and fiber bandwidth

Optical loss or attenuation in fibers is another wavelength dependent physical quantity that includes contributions from three major sources - material absorption, scattering, and confinement loss in the fiber at various circumstances such as structural imperfections, bending, splicing etc. Thus, the total propagation loss in fiber can be expressed as the sum of the material loss α_{mat}, loss from Rayleigh scattering α_R, and the confinement loss α_{wg} that includes the leakage of light from the fiber. However, the material absorption and Rayleigh scattering are the most dominant factors which eventually lead to optical power loss during transmission and hence loss of information carried by that pulse. Estimation of loss in fibers is carried out by the relation between the input power P_0 and the output power $P(z)$ at any length z given as,

$$P(z) = P_0 \exp[-\alpha z] \tag{1.20}$$

where α is the attenuation constant in units of m^{-1} which accounts for the total loss in the fiber from all sources. Using equation (1.20), it is easy to estimate the transmitted power at the output of a fiber of length L, provided the total fiber loss is known. It is customary to represent the attenuation constant in units of dB per unit length such that,

$$\alpha_{dB} = -\frac{10}{L}\log\left[\frac{P(z)}{P_0}\right] = 4.343\alpha. \tag{1.21}$$

The dominant contribution in fiber loss comes from the material used to fabricate the fiber through the imaginary part of the complex material refractive index. Through the Kramers-Kronig relation, the real and the imaginary part of the complex refractive index are related as,

$$n = n_{re} + i\kappa, \tag{1.22}$$

where κ is known as the extinction coefficient which is related to the attenuation coefficient α_{mat} by the expression,

$$\alpha_{mat} = \frac{4\pi\kappa}{\lambda}, \tag{1.23}$$

where λ is the wavelength of light used. It has already seen in equation (1.2) that material refractive index is a function of wavelength, and thus κ also varies as the wavelength changes. Equation (1.23) explicitly states that α_{mat} is also a wavelength dependent quantity, and one may experimentally obtain the absorption spectrum of a particular material. The attenuation from material absorption can be reduced by choosing materials exhibiting low absorption peaks within the transmission bandwidth of the waveguide. In this context, a transmission bandwidth of a fiber is the spectral range over which the optical power can be transmitted with minimum attenuation.

Further, the Rayleigh scattering is the second dominant mechanism contributed to fiber loss that arises from the density fluctuations frozen inside the glass during its fabrication resulting in local fluctuations in the refractive index of the glass material. Light gets scattered in all directions due to such local fluctuations and the loss associated with this scattering is proportional to λ^{-4}. Thus, it eventually becomes dominant in the lower wavelength regime. Moreover, due to the intrinsic nature of this loss contribution, it puts limit on the total transmitted power. It can be estimated as,

$$\alpha_R = \frac{C_R}{\lambda^4} \tag{1.24}$$

where C_R is a constant that depends on the fiber core constituents. However, the effect of Rayleigh scattering can be reduced by the state-of-the-art material purification processes which facilitate the fabrication of ultra-low loss fibers.

Finally, it is important for an optical fiber to estimate the loss contribution from the waveguide structure which is often referred to as confinement loss. It is to mention here that the fibers, where light is guided by the conventional total internal reflection (TIR) method, exhibit strong light confinement compared to the losses in fibers with light guidance mechanism other than TIR. Precisely, the confinement loss becomes dominant for photonic crystal fibers where the fiber modes are leaky in nature. The estimation of fiber confinement loss is performed by ignoring the extinction coefficient of the refractive index. In that case, the imaginary part of the complex effective refractive index n_{eff} associated with the fiber mode provides the amount of waveguide loss by the relation,

$$\alpha_{wg} = 8.686\frac{2\pi}{\lambda}\,\mathrm{Im}[n_{eff}]. \tag{1.25}$$

The amount of α_{wg} depends on the waveguide specifications like core radius, dimensions of microstructures in the cladding etc. and can be controlled by a judicious waveguide design that essentially contributes to the total loss minimization process.

Among other types of losses in fibers, bending loss and the loss due to scattering at the core-cladding interface may be accounted for specific cases. However, there are some fiber geometries specially designed for bend-insensitive light transmission. Furthermore, there is another source of absorption with a nonlinear origin. For very high intensity ultrashort pulses, some photons gets absorbed in the material. In that case, the absorption coefficient α becomes,

$$\tilde{\alpha}(\omega) = \alpha(\omega) + \alpha_2|E|^2, \tag{1.26}$$

where, $\alpha(\omega)$ is the linear absorption part, $|E|^2$ is the light intensity, and α_2 is known as the two-photon absorption coefficient. However, this absorption phenomena due to its nonlinear nature is material specific, and is triggered only if the photon energy is at least half the bandgap energy of the material.

In view of the various contributions to the total propagation loss, it is explicit that there is a limitation on the fiber transmission bandwidth strongly dictated by the amount of various losses over the specific range of wavelength. For transform-limited pulses, the spectral width can be estimated as $\Delta\omega = 1/T_0$ where T_0 is the initial pulse width. Thus, smaller the pulse width, wider will be the pulse spectrum. If the low-loss transmission bandwidth of the fiber is not sufficiently wide compared to $\Delta\omega$, then it essentially puts detrimental challenges on the pulse evolution over long distance. In general, the low loss region in the transmission bandwidth remains limited within a few tens of nanometer wavelengths. Ultrashort pulses with large spectrum suffer this narrow low-loss bandwidth leading to unwanted power loss and distortions during their transmission.

1.3 Optical pulse reshaping for stable delivery

It has been mentioned that ultrashort optical pulses suffer the dispersion and nonlinearity in a destructive manner, and their stable guided delivery is only possible if one can manage to reduce these effects. It is customary to design waveguides with insignificant effect of these physical factors during pulse propagation. However, these effects may also be distributed over propagation length where dispersive and nonlinear phase accumulations over each length-step will always limit the maximum stable propagation length of the ultrashort pulses. In that case, pulse distortion can be prevented by pulse reshaping technique where the shape, width, and amplitude of optical pulses can be controlled owing to certain conditions of dispersion and nonlinearity. Such pulse reshaping approach spawns a class of optical pulses that are conditioned in a way to be distortion free under any perturbation once formed, and are eventually advantageous for long distance delivery of ultrashort pulses. Moreover, the optical fiber based formation and stable delivery of such special pulses is the partial aim of this thesis. Thus, based on the sign of the fiber GVD parameter (β_2), two different pulse reshaping techniques will be discussed in the subsequent sections.

1.3.1 Soliton formation

Optical solitons are widely studied and practically exploited robust pulse form that can be generated in fibers with a delicately balanced anomalous dispersion (i.e. $\beta_2 < 0$) and nonlinearity. Earlier, it was seen that a continuous wave readily breaks into a train of pulses in the presence of anomalous dispersion and SPM. To understand this phenomena, one may consider the pulse

propagation equation neglecting the loss term given by Agrawal [2019d],

$$i\frac{\partial A}{\partial z} = \frac{\beta_2}{2}\frac{\partial^2 A}{\partial T^2} - \gamma|A|^2 A. \tag{1.27}$$

where, $\beta_2 < 0$ represents the anomalous dispersion regime, and γ is the nonlinear parameter. Moreover, let us consider the particular solution of the equation (1.27) as,

$$A = (\sqrt{P_0} + a)\exp[i\phi_{NL}], \tag{1.28}$$

where a is assumed to be a small perturbation added to the steady state solution of equation (1.27) with peak power P_0. Using equation (1.28), one readily obtains a propagation equation involving the perturbation term a only, whose solution leads to the dispersion relation,

$$K = \pm\frac{1}{2}|\beta_2\Omega|[\Omega^2 + \mathrm{sgn}(\beta_2)\Omega_c^2]^{1/2} \tag{1.29}$$

where K and Ω are the wave number and the frequency of the perturbation, respectively, and $\Omega_c = \frac{4\gamma P_0}{\beta_2}$. When $\beta_2 < 0$, $|\Omega| < \Omega_c$, and K becomes imaginary. This leads to an exponential growth of the perturbation a with z leading to an instability condition of light well-known as modulation instability. However, under certain conditions such instability eventually forms a group of pulse-like solutions that either do not change their shape or follow a periodic evolution pattern. By introducing a set of dimensionless parameters in equation (1.27),

$$U = \frac{A}{\sqrt{P_0}}, \qquad \xi = \frac{z}{L_D}, \qquad \tau = \frac{T}{T_0}, \tag{1.30}$$

and, replacing the pulse amplitude by $u = NU$, where, $N^2 = L_D/L_{NL}$ known as soliton order, the equation (1.27) becomes,

$$i\frac{\partial u}{\partial \xi} + \frac{1}{2}\frac{\partial^2 u}{\partial \tau^2} + |u|^2 u = 0. \tag{1.31}$$

Equation (1.31) can be solved by inverse scattering method, which leads to the general form of solutions,

$$u(\xi,\tau) = -2\sum_{j=1}^{N}(\sqrt{c_j}\exp\big(i\zeta_j\tau + i\zeta_j^2\xi\big))^*\psi_{2j}^* \tag{1.32}$$

where, ζ_j are the complex eigenvalues. Moreover, ψ_{2j}^* can be obtained by solving a set of linear algebraic equations. Making appropriate substitutions in (1.32), the general solution for the fundamental soliton with soliton order $N = 1$ is found to be,

$$u(\xi,\tau) = \eta\,\mathrm{sech}[\eta(\tau - \tau_s + \delta\xi)]\exp\big[i(\eta^2 - \delta^2)\xi/2 - i\delta\tau + i\phi_s\big], \tag{1.33}$$

where η represents the amplitude of the soliton, δ is the frequency, τ_s represents the position, and ϕ_s is the phase of the soliton. The dependence of the soliton solution on these four parameters can be reduced to a single parameter dependence by setting appropriate assumptions such as, $\phi_s = 0$ since its a constant absolute phase, $\tau_s = 0$ by choosing the position of the soliton peak at $(\tau = 0, \xi = 0)$, and $\delta = 0$ by choosing an appropriate carrier frequency. Thus, the form of the fundamental soliton becomes,

$$u(\xi,\tau) = \eta\,\mathrm{sech}(\eta\tau)\exp\big(i\eta^2\xi/2\big). \tag{1.34}$$

In equation (1.34), the parameter η determines both the amplitude and the width of the soliton. In general, soliton width changes with η as T_0/η i.e., it scales inversely with soliton amplitude. Formation of such pulses in fibers requires strict dispersive and nonlinear phase cancellation in such a way that they acquire a particular width and amplitude which is maintained throughout. In this process, energy of the initial pulse do not remain conserved, but gets dissipated to reshape into a soliton. There are different orders of solitons based on N among which the fundamental one is of utmost importance and will only be considered later in this study. An evolution of fundamental soliton in a fiber has been shown in figure 1.3(a).

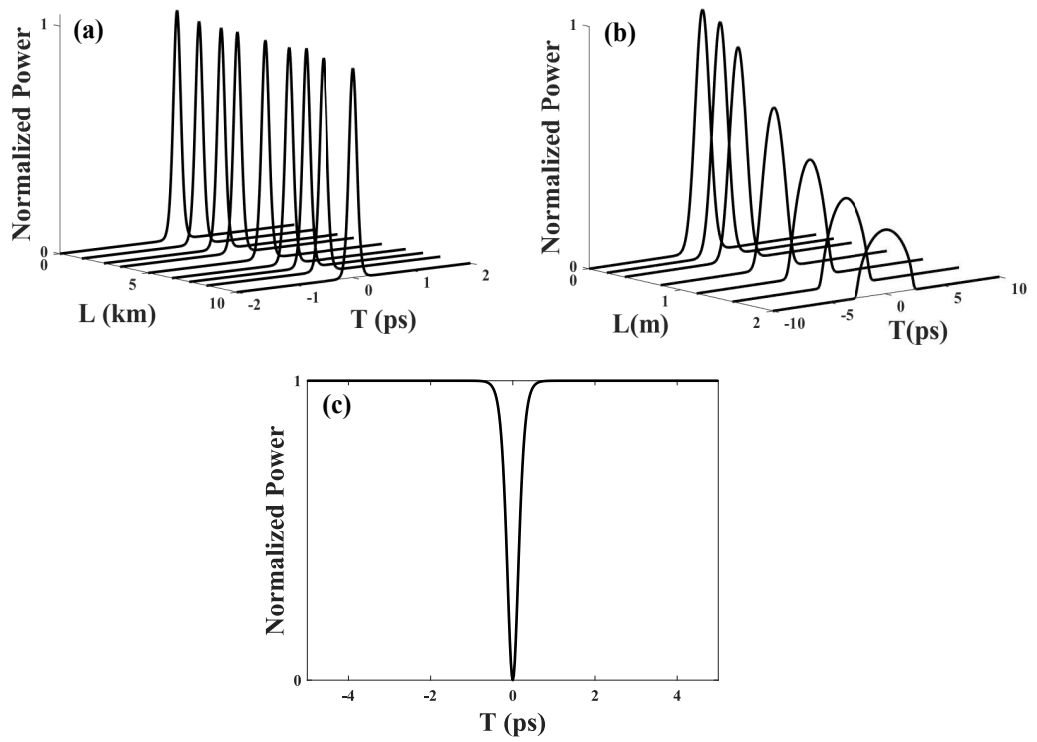

Figure 1.3: (a) Evolution of soliton from a sech input pulse form inside a 10 km long optical fiber, (b) Evolution of parabolic pulse from a Gaussian pulse as input through a 2 m long dispersion decreasing fiber, and (c) a dark similariton pulse with infinite background.

1.3.2 Similariton formation: Parabolic pulse and Dark similariton

Similaritons are a group of optical pulses that evolve through the fiber self-similarly and thus maintain their shape throughout the propagation distance without any distortion. Formation of such self-similar pulses usually occurs in presence of positive GVD parameter i.e. $\beta_2 > 0$ (as known as normal GVD) and strong nonlinearity with some physical conditions satisfied. Precisely, the development of a time-dependent phase change during the pulse propagation explains the phenomenon of pulse distortion as well as the origin of the breaking-free pulses inside the fiber [Tomlinson et al., 1985; Anderson et al., 1993]. Considering any standard initial pulse shape with or without an initial phase variation, the accumulated phase inside the pulse has found to be quadratic in nature at any fiber length. Such quadratic phase eventually gives rise to an instantaneous frequency that differs from the pulse central frequency. A time-derivative of the phase results in a linear dependence of the frequency with time, and is referred as frequency chirp defined by the expression,

$$\delta\omega = -\partial\phi/\partial t, \tag{1.35}$$

where, ϕ is the total phase associated with the propagating pulse. In a normally dispersive nonlinear fiber, $\delta\omega$ consists of both the linear frequency chirp induced through normal GVD, and the nonlinear frequency chirp induced through SPM. A mathematical observation reveals that the frequency chirp $\delta\omega$ is proportional to the ratio γ/β_2, a smaller value of which should develop a monotonically varying chirp, whereas a larger value gives rise to non-monotonic chirp variation. The monotonic chirp implies that the various pulse parts in the leading edge are propagating with increasing velocity in forward direction, and vice-versa for the trailing edge, with no overlapping between different pulse components. Presence of such monotonic chirp preserves pulse form during evolution, and thus is of utmost importance. It can be further explained by considering two pulse parts separated

by a time-separation $\Delta\tau$. As the pulse propagates down the fiber, $\Delta\tau$ will be varying due to the different velocities of the two pulse parts originated from the frequency chirp variation. If the pulse is assumed to propagate a distance z, then the time separation between the two pulse parts at z will be given by [Anderson et al., 1992],

$$\Delta\tau' \approx z\frac{d^2\beta}{d\omega^2}\frac{d(\delta\omega)}{d\tau}\Delta\tau, \tag{1.36}$$

where $d^2\beta/d\omega^2$ accounts for dispersion. For a monotonic chirp variation, the rate of change of time-separation i.e., $\Delta\tau'/\Delta\tau$, should be equal for all pulse parts. However, the situation becomes different for high intensity short optical pulses in presence of normal GVD and nonlinearity. In general, the characteristic of normal GVD is to decrease the group velocity with increasing frequency, and vice-versa. Moreover, a high intensity short pulse is prone to the SPM-induced spectral broadening, where new frequencies are generated at the edges of the pulse spectrum. The simultaneous action of normal GVD on the newly generated frequencies speeds up the lower frequency components and slows down the higher frequency components. As a result, the frequency chirp exhibits a non-monotonic variation with time at the pulse edges, and the shifted frequency components in the pulse' leading and trailing edges overrun the unshifted frequency components across the pulse center. This series of phenomena is originated when in equation (1.36), $\Delta\tau' = -\Delta\tau$ is satisfied for some τ. Thus, interference occurs between different frequency components leading to the broadening of the pulse in time-domain with fine oscillations at pulse edges which further results in gradual pulse degradation and optical wave-breaking (OWB).

Interestingly, such wave-breaking due to nonlinear frequency generation can be prevented with a monotonous frequency chirping where $d(\delta\omega)/d\tau$ is independent of time τ. Hence, it preserves the pulse form and helps it to evolve self-similarly. On rigorous analysis, it has been observed that the evolution of $\delta\omega(\tau)$ over the fiber length z can be approximated by [Anderson et al., 1993],

$$\delta\omega(z,\tau) \approx \delta\omega(0,\tau) + \frac{\partial}{\partial\tau}\left(\frac{\beta_2}{2}\left[\frac{1}{A(0,\tau)}\frac{\partial^2 A(0,\tau)}{\partial\tau^2} - \delta\omega^2(0,\tau)\right] + \gamma A^2(0,\tau)\right)z, \tag{1.37}$$

where $A(0,\tau)$ and $\delta\omega(0,\tau)$ are the initial pulse amplitude and frequency chirp. Considering an initially unchirped pulse, $\delta\omega(0,\tau) = 0$, and the requirement for monotonic chirp that $d(\delta\omega)/d\tau$ is independent of time τ, yields the following condition on the initial pulse form,

$$\frac{\beta_2}{2}\frac{1}{A(0,\tau)}\frac{\partial^2 A(0,\tau)}{\partial\tau^2} + \gamma A^2(0,\tau) = C_0 + C_1\tau^2, \tag{1.38}$$

where it has assumed that $A(0,\tau)$ is an even function of τ, and C_0 and C_1 are constants. From equation (1.38), three different cases can be observed explicitly. First, if $C_1 = 0$, then it yields solutions of solitary waves those not only preserve their shapes but also remain invariant. Second, with $\gamma = 0$ one obtains linear pulse evolution with dispersion induced broadening. Third, in presence of both β_2 and γ, only a few particular pulse forms with high intensity exhibit the important feature of having monotonic frequency chirp. Analysis has revealed that a parabolic pulse form expressed as,

$$A^2(0,\tau) = A_0^2\left(1 - \frac{\tau^2}{\tau_0^2}\right), \tag{1.39}$$

where A_0 and τ_0 to be the pulse amplitude and width, respectively, is one of the breaking-free pulses well-satisfying the condition of time-independent frequency chirp variation. Their formation occurs at an asymptotic limit of propagation i.e. $z \to \infty$ with an uniform longitudinal dispersion profile and distributed gain or loss. Moreover, having a longitudinally decreasing dispersion profile in an all-lossy environment is another approach of pulse reshaping in longitudinally tapered fibers that

renders an equivalent role of gain in fiber amplifiers. Such formation of parabolic pulses from an initial Gaussian pulse inside a tapered fiber is depicted in figure 1.3(b). Parabolic pulses formed by all these techniques essentially develop linear chirp across the entire pulse width during its evolution through a normally dispersive fiber and can withstand strong nonlinearity without wave-breaking. It is to mention here that the self-similar parabolic evolution is entirely dependent on the initial pulse energy, rather than shape of the pulse, which essentially dictates the width and amplitude of the pulse at each step of evolution. It means that all of the input pulse forms with same energy will reshape into a parabolic pulse with linear chirp under suitable dispersive and nonlinear environment in an asymptotic limit.

On the other hand, there is a group of exact self-similar solution of the pulse propagation equation governing nonlinear dynamics of optical pulses in fibers [Kruglov et al., 2003]. In that case, all the fiber parameters such as dispersion, nonlinearity, and gain/loss are assumed to be distributed over the entire fiber length i.e., β_2, γ and g or α are varying functions of length z. To yield a self-similar solution of the pulse propagation equation with quadratic phase, a necessary and sufficient condition between the fiber parameters $\beta_2(z)$, $\gamma(z)$, and $g(z)$ has to be maintained:

$$g(z) = \frac{1}{\rho(z)}\frac{d}{dz}\rho + \frac{2c_0\beta_2(z)}{1 - c_0 D(z)}, \tag{1.40}$$

where $\rho(z) \equiv \beta_2(z)/\gamma(z)$, $D(z) = 2\int_0^z \beta_2(z')dz'$, and c_0 is a nonzero integration constant. As a result, linearly chirped similaritons are formed with hyperbolic secant (sech) and hyperbolic tangent (tanh) pulse forms. For $\beta_2(z)\gamma(z) < 0$, A *sech* pulse form is obtained given by,

$$A(z,\tau) = \frac{\sqrt{|\rho(z)|}}{\tau_0(1 - c_0 D(z))}\,\mathrm{sech}\left(\frac{\tau - \tau_c}{\tau_0(1 - c_0 D(z))}\right), \tag{1.41}$$

where τ_0 is the pulse width, and τ_c is the pulse center. Solutions of the form given in equation (1.41) are called bright similaritons. For $\beta_2(z)\gamma(z) > 0$, solutions of the following form are obtained,

$$A(z,\tau) = \frac{\sqrt{|\rho(z)|}}{\tau_0(1 - c_0 D(z))}\,\tanh\left(\frac{\tau - \tau_c}{\tau_0(1 - c_0 D(z))}\right), \tag{1.42}$$

and are called dark similaritons. Generally, the dark similaritons are considered as kink solutions in an infinite continuous background as shown in figure 1.3(c). In this thesis, we will focus only on the solutions of dark simiaritons with a finite compact background.

1.4 Specialty optical fibers for high power ultrashort pulse propagation

It has already been mentioned in the previous section that the optical fiber based pulse reshaping technique requires delicate balance between the fiber parameters. In some cases, it also requires a length-dependent variation of parameters to achieve proper reshaping, and here lies the efficiency of fibers which allow a fiber engineer to tailor the essential features as suitable. However, a typical TIR-based step-index fiber eventually falls short when it comes to fiber engineering schemes. In that case, one has to lean on special fiber structures based on light guidance mechanisms that are away from the conventional TIR guidance. Photonic crystal fibers (PCF) are a group of special waveguide geometries that allows light to be guided via either modified index-guided mechanism or bandgap formation method. Importantly, such fibers readily provide ample degrees-of-freedom to tailor fiber parameters through appropriate fiber design and facilitate the process of distortion-free pulse delivery for targeted specialty applications. Thus, they are often termed as specialty optical fibers. On the other hand, there are certain photonic crystal based waveguides that confines light

via band-topology. Unlike bandgap fibers, the mechanism of light confinement in such topological waveguides depends on the geometric properties of the bands rather than the properties of the bandgaps. Such topology protected light states exhibit robust transmission through the waveguide and are readily useful for next-generation guided photonic systems.

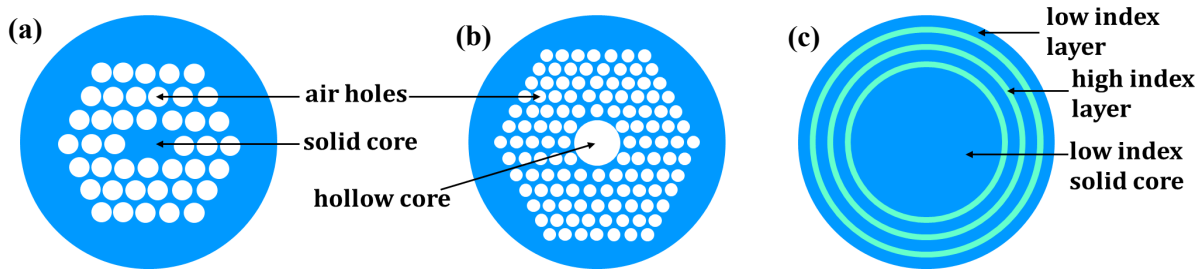

Figure 1.4: The schematic representation of (a) index guided PCF, (b) hollow-core bandgap guided PCF, and (c) all-solid Bragg fiber.

1.4.1 Photonic crystal fibers fundamentals: index guided and bandgap guided fibers

Photonic crystal fibers (PCF), also termed as microstructured fibers, comprises of periodically arranged tiny structures with dimensions in micron or sub-micron range either embedded within or surrounding a homogeneous matrix. These may commonly be understood as fibers made up of conventional photonic crystals in one/two-dimensions in the transverse cross-section and running along the fiber length with a central defect that forms the fiber core. PCFs exhibit two prime light guiding principles - i) index guidance or modified TIR, and ii) photonic bandgap guidance, based on the geometry and index profile of the fiber cross-section.

i) Index guided PCFs: Such PCFs comprises of periodically arranged air-holes or holes filled with very low-index material embedded in a high-index matrix as shown in figure 1.4(a). Removal of one or more holes from the center of the structure creates a high-index defect region where light gets confined owing to the index guiding mechanism, often known as modified TIR effect [Joannopoulos et al., 2008]. In that case, the periodic arrangement of low-index holes is introduced to reduce the effective refractive index of the cladding region surrounding the high-index core rather than creating a bandgap. Moreover, the guided modes are the discrete sets of solution that lie below the light line in the energy dispersion relation or the band diagram ($\omega - k_z$ curve) corresponding to the fiber geometry and decays exponentially away from the core. These fibers are readily suitable for tailoring the fiber dispersion parameter as well as number of guided modes in the fiber. Endlessly single mode operation is an important application of such PCFs.

ii) Photonic bandgap guided PCFs: In such fibers, light gets confined in a low-index core via photonic bandgap formation. The cross-section of these PCFs are somewhat similar to the index-guided one with the exception that the fiber core is either hollow or filled with relatively low-index material than the refractive indices of the photonic crystal based cladding region. The periodic arrangement of high and low index layers in the cladding essentially forms the photonic bandgap. Thus light with frequencies lying within the bandgap will be guided through the low-index fiber core. In that case, there are two possibilities of bandgap guidance; one occurs through a two-dimensional (2D) photonic crystal geometry (as shown in figure 1.4(b)) in the cladding that essentially supports bandgap guided modes in the hollow core which lies above the light line in the $\omega - k_z$ curve; the other one occurs through Bragg reflections from one-dimensional (1D) cylindrical periodic high/low-index layers (figure 1.4(c)) forming 1D bandgaps to guide modes in the low-index core [Joannopoulos et al., 2008]. 2D Hollow-core PCFs are widely studied and exploited for their

negligible nonlinearity, and customizable dispersion. However losses can be relatively large in such fibers due to the overlapping of the core modes and the cladding modes, and their delicate geometry pose a challenge towards accurate fabrication and performance. Besides, the 1D bandgap fibers can be made available with hollow core as well as solid low-index core, and possess more flexibility in terms of fiber engineering with ample structural robustness.

1.4.2 1D Photonic bandgap fibers: Bragg fibers

Bragg fibers are 1D bandgap fibers where a periodic multilayered film composed of alternate high and low index material acts as a cladding surrounding a low-index or hollow fiber core. The schematic of the Bragg fiber cross-section is shown in figure 1.4(c). If the index contrast of the cladding dielectrics is large enough then one can easily employ a simpler asymptotic approximation method for modal analysis. But such approximation method fails when the index contrast is lower and one should use transfer matrix method with scalar approximation to analyze the modes of the fiber. It is explicit from the cross-sectional geometry of Bragg fibers that it holds a rotational symmetry in the ϕ direction, along with the translational symmetry along the fiber length z, and thus the electric field of an eigenstate can be written in the separable form [Joannopoulos et al., 2008],

$$E_{k_z,m} = e^{ik_z z + im\phi} E_{k_z,m}(r) \tag{1.43}$$

where k_z is the wave vector along z, m is the angular mode number, $E_{k_z,m}(r)$ is the modal field which has only radial dependence and thus it has reduced to a one-dimensional problem. Under scalar approximation, $E_{k_z,m}(r)$ will satisfy the following differential equation describing the radial part of the modal field,

$$r^2 \frac{d^2E}{dr^2} + r\frac{dE}{dr} + [(k_0^2 n_p^2 - \beta^2)r^2 - m^2]E(r) = 0, \tag{1.44}$$

where, $k_0 = 2\pi/\lambda$, n_p is the refractive index of the pth layer, β the propagation constant, and m is azimuthal mode number. The solution of equation 1.44 can be obtained by employing a numerical approach based on transfer matrix method (TMM) as described in [Thyagarajan et al., 1991]. The details of the TMM and the modal solutions of Bragg fibers will be discussed in chapter 3.

The multilayered cladding of these fibers surrounding the low-index core (hollow or solid) essentially works as a Bragg mirror which reflects back light of certain frequencies that lies in the photonic bandgap of the layered medium. The formation of the photonic bandgap is similar to that happens in case of a 1D periodic layered structure. Assuming the EM wave with a periodicity along x direction only, the field can be written in the form of Bloch waves given by [Yariv and Yeh, 2007],

$$\mathbf{E} = E_K(x) e^{-iKx} e^{i\omega t - k_y y} \tag{1.45}$$

where, $E_K(x) = E_K(x + \Lambda)$ is the periodic part of the wave, Λ to be the unit cell of the structure composed of a high-index and a low-index layer with thicknesses d_1, d_2, respectively, such that $\Lambda = d_1 + d_2$, and K is the Bloch wave number. From the condition of periodicity of the structure, and from the condition of continuity between two consecutive unit cells, one eventually achieves the eigenvalue equation for the Bloch waves to be,

$$\begin{bmatrix} A & B \\ C & D \end{bmatrix} \begin{bmatrix} a_n \\ b_n \end{bmatrix} = e^{iK\Lambda} \begin{bmatrix} a_n \\ b_n \end{bmatrix} \tag{1.46}$$

where a_n, b_n are the constants related by the continuity condition at the interface of two unit cells, and $e^{iK\Lambda}$ is the eigenvalues of the unit cell translation matrix (A, B, C, D), which is expressed as,

$$\cos K\Lambda = \frac{1}{2}[A + D]. \tag{1.47}$$

From equtaion (1.47), the dispersion relation between the frequency ω, wave vector k_y, and the Bloch wave number K is obtained as,

$$K(\omega, k_y) = \frac{1}{\Lambda} \cos^{-1}\left[\frac{A+D}{2}\right]. \tag{1.48}$$

When $|(A+D)/2| > 1$, then K becomes imaginary making the Bloch waves evanescent. This forms the photonic bandgaps of the 1D periodic layers. Specific band-diagrams (ω vs k_y plot) for a particular cross-section of the Bragg fiber can be obtained by solving equation (1.48). In general, the bandgaps of 1D multilayered structures with large radius of curvature i.e., $r \to \infty$ are such that if any state of light with frequency ω and wave vector k_z falls within the 1D bandgap, it will be confined to the core. However, photonic bandgap fibers are leaky structures in a sense that there are always an evanescent field exists in the multilayered cladding. The core is specifically designed to host resonances which falls within the stop band of the cladding geometry by using the relation,

$$r_c k_c = 2\pi, \qquad \text{where} \qquad k_c = k_0\sqrt{n_c^2 - n_{eff}^2} \tag{1.49}$$

where, r_c is the core radius, and n_c is the refractive index of the core, and n_{eff} is the effective refractive index of the mode. Moreover, as the modes of Bragg fibers are leaky in nature, it requires large number of cladding layers to obtain strong confinement. In that case, the confinement of the fundamental mode can be made stronger by estimating the cladding layer thicknesses d_1 and d_2 using the quarter wave stack condition given by [Ghosh et al., 2011],

$$k_1 d_1 = k_2 d_2 = \frac{\pi}{2} \tag{1.50}$$

where $k_i = k_0\sqrt{(n_i^2 - n_{eff}^2)}$; $i = 1, 2$. Similarly, for the first higher order mode i.e., $l = 1$, the condition for anti-reflection becomes,

$$k_1 d_1 = k_2 d_2 = \pi. \tag{1.51}$$

Bragg fibers are readily useful for easy tailoring of fiber parameters including dispersion, nonlinearity, and fiber loss owing to their unique multilayered structure and light guidance principle. Lately, various bio-medical applications like laser surgery, endoscopy etc. use the hollow-core Bragg fibers for high power delivery. However, compared to its hollow-core counterpart as well as any other PCFs, the all-solid Bragg geometry are somewhat less-explored fiber structure that provides more flexibility towards novel specialty fiber designs with profound efficiency for targeted applications, and therefore has been chosen as the basic waveguide model in this chain of research.

1.4.3 Topological waveguides, band-topology and towards 1D topological fiber

In recent years, a massive exploration of topological phases in photonic systems, which is directly related to their photonic bandgap structure, has introduced some exclusive states of light. Having the striking similarity of bandgap structures of photonic crystals with the electronic bandgaps, topological phases and the exquisite phase transition phenomenon have been studied and developed in photonic crystals and photonic crystal based waveguides in all dimensions [Ozawa et al., 2019]. It is well-known that light, propagating through photonic crystals with periodically layered dielectrics, yields the solutions of Maxwell's equations in the form of Bloch functions given by,

$$\psi_{n,k}(\mathbf{r}) = e^{i\mathbf{k}.\mathbf{r}} u_{n,k}(\mathbf{r}) \tag{1.52}$$

where n is the band index, k the momentum vector within the first Brillouin zone, and $u_{n,k}$ is the periodic part of the Bloch function or simply the eigenstate of the nth band with wave vector

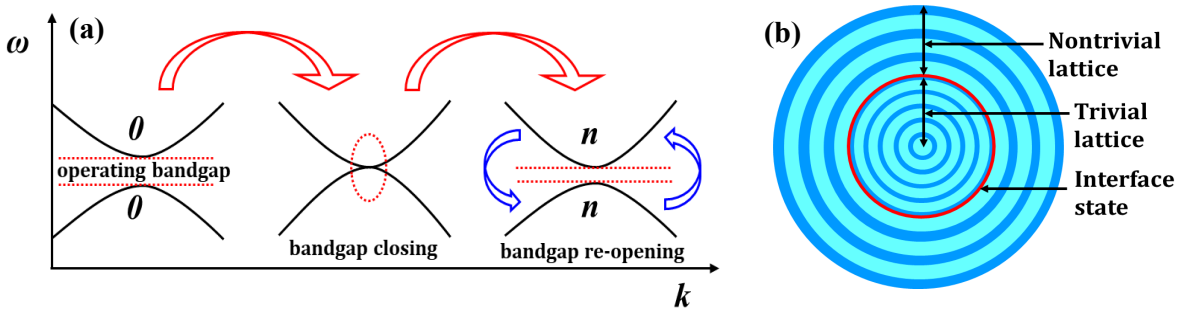

Figure 1.5: (a) The schematic representation of topological phase transition. The red arrows denote the sequential closing and re-opening of the operating bandgap under perturbation. The blue arrows denote the phase transition between the two bands adjacent to the operating bandgap. Also, the topological invariants of the bands are shown before and after the phase transition. (b) The schematic of the topological fiber cross-section based on 1D periodic lattice along with the interface state.

k. Precisely, the physical properties of an energy band is partly retained in the energy dispersion relation obtained by solving the Bloch Hamiltonian, and partly encoded as a geometric phase resulting from an adiabatic translation of all the eigenstates $u_{n,k}$ in the energy band n over a closed path through the entire momentum space $\mathbf{k}$ defined by the first Brillouin zone. These geometric phases associated with each energy band are referred as the topological phases of photonic bands, known as Berry phase, and is obtained by the closed path integration,

$$\gamma_n = \oint A_n(\mathbf{k}) \cdot d\mathbf{k}, \tag{1.53}$$

where $A_n(\mathbf{k})$ is termed as Berry connection and is defined as,

$$A_n(\mathbf{k}) \equiv i \langle u_{n,k} | \boldsymbol{\nabla} | u_{n,k} \rangle . \tag{1.54}$$

A topologically invariant quantity can be derived from the Berry phase that exclusively defines the topology of the system. However, it is important to note that the Berry connection is not invariant under a gauge transformation, and thus it is necessary to define a gauge-invariant quantity, known as Berry curvature, defined as,

$$\Omega_n(\mathbf{k}) = \boldsymbol{\nabla}_n \times A_n(\mathbf{k}), \tag{1.55}$$

which encodes the geometrical properties of the nth band. In that case, $\Omega_n(\mathbf{k})$ can be continuously defined over the whole Brillouin zone. However, the phases of the Bloch states may not be chosen to be continuous always, and thus it is required to define a topological invariant of the band defined by the integral,

$$C_n = \frac{1}{2\pi} \int_{BZ} \Omega_n(\mathbf{k}) d^3k \tag{1.56}$$

over the first Brillouin zone, known as Chern number, to extract information about the continuity of the Bloch states. If the invariant quantity i.e., C_n has a value '0' and remains strictly constant under smooth perturbation, then the system is said to have a trivial topology where the Bloch states can be defined continuously. On the other hand, a nonzero value of the topological invariant C_n results in a nontrivial topology where the Bloch states and hence the Berry connection can not be defined continuously. In such nontrivial systems, topological phase transition occurs through a bandgap closing and reopening process and is depicted in figure 1.5(a) where the phases of

the bands adjacent to a particular bandgap are switched. There are ample amount of work in the literature that have described the topological phase transition in exclusive photonic crystal structures that necessarily involve breaking of certain symmetry like time-reversal symmetry and inversion symmetry [Haldane and Raghu, 2008; Kim et al., 2020]. The ultimate motif is to obtain a robust state of light that encounters strong insulation in the bulk of both the trivial and nontrivial counterparts, and localized entirely at the interface of the two, a concept primarily originated from the bulk-edge correspondence theory. These interface states of light have their frequency lying in the bandgap of the topologically distinct systems around which the phase transition has occurred, and are truly interesting for back-reflection free, one-way propagation of light. While a 2D photonic crystal based waveguide structure with broken time-reversal and inversion symmetry is more convenient to study the dynamics of interface light states [Rechtsman et al., 2013a; Kim and Rho, 2020; Kim et al., 2020], the 1D geometry does require some modifications to induce phase transitions. There are some special topological models in 1D like Su-Schrieffer-Heeger (SSH) model [Malkova et al., 2009; Zhao et al., 2018] and Aubrey-André-Harper (AAH) model [Pilozzi et al., 2020] that typically contain some chiral and inversion symmetry to break. Besides, a simple periodic 1D photonic crystal exhibits only the inversion symmetry and can provide back-reflection free interface states via accurate design of the trivial and nontrivial crystals [Xiao et al., 2014a; Ota et al., 2018]. It is important to mention here that in 1D bandgap structures, the topological invariant is no longer defined by Chern number; instead it is quantified by a separate definition known as *Zak phase* expressed as [Zak, 1989],

$$\theta_n = \int_{-\pi/a}^{\pi/a} \left(\frac{2\pi}{a} \int_0^a u^*_{n,k}(z) i \frac{\partial}{\partial k} u_{n,k}(z) dz \right) dk, \tag{1.57}$$

where, a is the lattice constant. Based on the periodic 1D geometry, topological waveguides in cylindrical form can be designed where light will be confined at the interface of the two topologically distinct layered structures as shown in figure 1.5(b). We may mention these multilayered cylindrical waveguides as 1D topological fibers, which has the same 1D photonic bandgap structure like Bragg fibers, but supports an entirely new way of band-topology based light guiding in optical fibers away from the conventional approaches.

1.5 A review on pulse reshaping and propagation in optical fibers

The concept of pulse reshaping started to develop about three decades back, when optical fibers had already established their ground as the potential global means of information transport. Communication system based on optical fiber was revolutionized with the introduction of the specific solitary waves known as optical solitons. On the other hand, researchers tried to come up with a solution to tolerate excessive nonlinearity in fibers overcoming the detrimental OWB and to achieve a sustained solution. With the first explanation of the OWB phenomenon during propagation of femtosecond pulses in a single mode fiber [Anderson et al., 1992], the domain of ultrashort pulse propagation and nonlinear fiber optics have indeed been revolutionized .

1.5.1 Soliton formations in optical fibers

To date, innumerable works have been reported in literature on fiber based generation of optical solitons and their exclusive varieties, among which only a brief review of them focusing on some recent progresses have been presented here. Optical solitons were first proposed for communication purpose, where the two researchers from Bell Lab, A. Hasegawa and F. Tappert, reported for the first time the presence of nonlinear stationary waves that are quite stable under noise and various fiber losses [Hasegawa and Tappert, 1973a,b]. Consequently, several experimental demonstrations

of distortion free fiber amplifier based soliton formation over long distances mostly targeted for optical communication purposes were reported in [Mollenauer et al., 1985; Mollenauer and Smith, 1988; Beaud et al., 1987; Mamyshev et al., 1991]. Moreover, extensive experimental and theoretical studies on the generation of bright solitons, multiple solitons, and soliton pulsating and their interactions in actively mode-locked fiber lasers [Deparis et al., 2001; Zhang et al., 1998; Malmström et al., 2012] as well as in passively mode-locked fiber lasers [Amrani et al., 2011; Liu, 2011; Tang et al., 2005; Niang et al., 2014; Wang et al., 2019b] have been widely reported. Also, there are numerous works in literature on the fundamental theory of fiber based generation of dark solitons, which are basically absence of light in a continuum, and their experimental observations has been extensively reported to date [Gredeskul and Kivshar, 1989; Weiner et al., 1988; Mahalingam and Porsezian, 2001; Song et al., 2014; Milián et al., 2009; Guo et al., 2015; Ge et al., 2015; Liu et al., 2019]. There are also other kinds of optical solitons like vector solitons, dissipative solitons, dispersion-managed solitons etc. which readily finds myriad applications in optical signal processing, bio-photonics, sensing and so on [Zhang et al., 2008; Jin et al., 2016; Ma et al., 2019; Hu et al., 2020; Renninger et al., 2008; Zhang et al., 2010; Zhang and Dai, 2011; Turitsyn et al., 2016; Peng et al., 2019; Li et al., 2022; Turitsyn et al., 2012]. Besides conventional fiber lasers and amplifiers, solitonic propagation of light has also been investigated both in solid core PCFs [Fedotov et al., 2009; He et al., 2015], as well as in hollow core PCFs [Welch et al., 2009; Saleh et al., 2011; Zhou et al., 2013; Ermolov et al., 2015; Xu et al., 2017; Hosseini et al., 2018; Sharma et al., 2019] for multiple purposes such as supercontinuum generation, slow light observation, low energy soliton formation etc.

1.5.2 Similariton formations in gain-assisted and passive optical fibers

Earlier it was a challenge to send high power short pulses through a very long fiber until the presence of certain wave-breaking free pulses have been introduced in nonlinear single mode fibers. Towards this, a detailed analytical formulations describing the features of the breaking-free pulses such as linear frequency chirp, and the parabolic pulse form that essentially hold those features have been reported. In 2000, M. E. Fermann *et. al.* were first to report the experimental observation of parabolic pulse formation and amplification in a high gain fiber amplifier that went exactly in agreement with the theoretical results reported so far [Fermann et al., 2000]. The group of researcher continued to report the detailed numerical observations of the generation and interaction of parabolic pulses in a normal GVD, high gain fiber amplifier in the asymptotic limit along with the crucial design specifications of the amplifier for similariton generation [Peacock et al., 2001; Kruglov et al., 2002; Finot et al., 2004]. Moreover, a numerical study on the formation of parabolic pulses in highly nonlinear Raman amplifier [Peacock et al., 2003], and the dependence of pulse reshaping on stimulated Raman process and gain bandwidth [Chang et al., 2004] have also been reported. In 2004, parabolic pulse formation in mode-locked Lasers has been investigated and reported numerically [Ilday et al., 2004]. Later in 2007, a detailed study on the parametric instability of the similariton mode-locked pulses in mode-locked fiber laser [Logvin and Anis, 2007], and a complete numerical analysis of the different mode-locking regimes for the laser-based formation of linearly chirped parabolic pulses [Schreiber et al., 2007] have been investigated and reported. Moreover, there are several reports on the generation of ultrashort parabolic pulses in various fiber lasers in [Prochnow et al., 2007; Oktem et al., 2010; Renninger et al., 2010; Aguergaray et al., 2010; Lefrancois et al., 2013; Liu et al., 2014; Tang et al., 2015; Ilday et al., 2003; Buckley et al., 2006; Zhou et al., 2008]. In a parallel time, the evolution of self-similar parabolic pulses in a normal dispersion decreasing fiber amplifier has been investigated and reported with a detailed analytical description for a better stability of the output pulses in amplifiers [Wabnitz and Finot, 2008]. In this direction, D. Ghosh *et. al.* have reported the self-similar evolution of parabolic pulses via presence of a virtual gain resulting from increasing nonlinearity along with physical gain in a silica based parabolic index normal dispersion decreasing fiber amplifier [Ghosh et al., 2009] along with a detailed theoretical

study on the performance of pulse reshaping in presence of macrobending at telecom wavelength [Ghosh and Basu, 2016]. Later, they showed an equivalent cascaded fiber profile with alternately arranged passive and active dispersion compensating fibers to form parabolic pulses within a very short optimum fiber length compared to their previously reported normal DDF amplifier [Ghosh and Basu, 2010]. Moreover, formation of parabolic pulses from femtosecond range of initial pulse width in normally dispersive Er-doped fiber amplifier with multiple cladding sections [Bose et al., 2013], as well as self-similar evolution of parabolic pulses through a silica based normal dispersion fiber amplifier with varying nonlinearity [Ghosh et al., 2015; Chowdhury et al., 2018] have been reported.

Beside the gain-assisted similariton generations, there are several reports on the formation of parabolic pulses in passive optical fibers. In 2004, Hirooka and Nakazawa have demonstrated for the first time a novel approach towards parabolic pulse formation in passive medium based fibers in presence of a decreasing dispersion profile [Hirooka and Nakazawa, 2004]. Later, the effects of loss and third order dispersion on the generation of high power parabolic pulses in dispersion decreasing fibers (DDF) has been reported with thorough analytical demonstration [Latkin et al., 2007; Zhang et al., 2009]. Recently, a technique to reduce the detrimental effect of TOD in normally dispersive DDF has been reported that uses an electro-optic phase modulator inside the fiber link as well as a dispersion shifted fiber with opposite sign of TOD replacing the phase modulator to suppress the TOD effect, and to regenerate parabolic pulses [Chowdhury et al., 2019]. In 2007, C. Finot *et. al.* have presented various possibilities of generation of parabolic pulses such as active and passive dispersion decreasing fibers [Finot et al., 2007a], and normally dispersive two-segment fibers [Finot et al., 2007b]. In 2008, C. Finot has reported the formation and stability of parabolic pulses in a dispersion managed fiber where both the normal and anomalous dispersion regimes exist periodically [Finot, 2008]. Further, various fiber geometries, such as fiber Bragg gratings [Parmigiani et al., 2006], Bragg-like chirped clad all-solid fibers [Ghosh et al., 2010], solid core photonic bandgap fibers [Nagaraju et al., 2010], index-guided microstructured fibers [Barh et al., 2014], all with dispersion decreasing profile have been exploited to achieve passive formation of parabolic pulses. Towards this, the stability analysis of passively formed parabolic pulses in a chalcogenide glass based tapered mictrostructured fiber has been reported exhibiting the intermediate transient state of the self-similar evolution in the highly nonlinear and highly dispersive environment [Biswas et al., 2016]. It is to mention here that the highly nonlinear decreasing dispersion profile often exhibit this transient state of pulse propagation where OWB occurs over long distance propagation. In this context, numerical and experimental observations on the passive formation of parabolic pulses with a uniform normal dispersion profile have been demonstrated in [Iakushev et al., 2012; Sukhoivanov et al., 2013] which essentially report a steady state regime of pulse propagation exceeding the OWB length beyond the transient state of evolution.

Furthermore, apart from the asymptotic pulse reshaping technique, there is another fundamental approach with normal disperion that leads to the exact solutions in the form of hyperbolic secant (sech; bright similaritons) and hyperbolic tangent (tanh; dark similaritons) functions embedded in infinite background, and they need delicate balance between fiber parameters such as dispersion, nonlinearity and fiber gain-loss [Kruglov et al., 2003; Soloman Raju et al., 2005; Ponomarenko and Agrawal, 2007; Wu et al., 2009].

1.6 Ultrashort pulses in linear time-varying media

A time-varying medium is one in which any of its inherent properties like dielectric constant ϵ or refractive index n will be a function of time t, instead of a function of space as in optical fibers. This thesis partially focuses on the study of the behavior of ultrashort pulses in such dynamic

systems in which the light states should essentially be of unique features like photon acceleration or deceleration that may be a challenge to observe in conventional space-modulated or static systems.

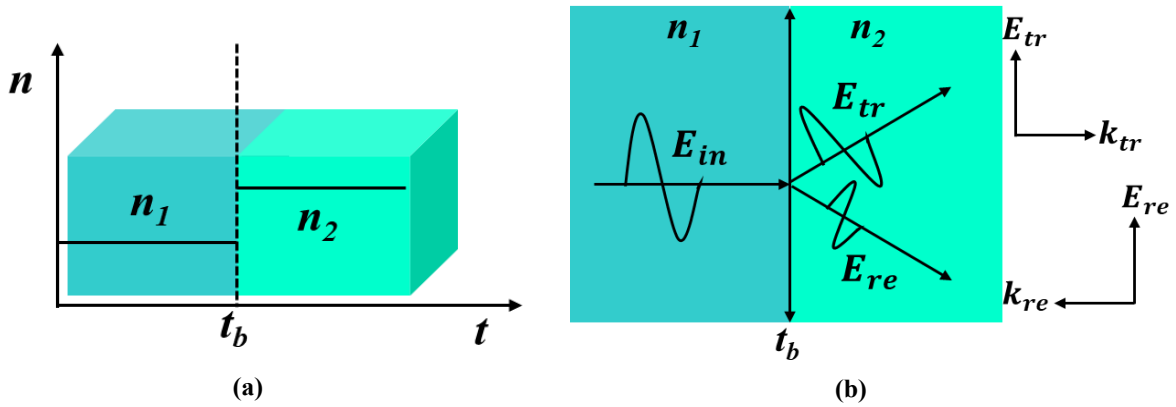

Figure 1.6: (a) The schematic representation of the linear time-varying medium in which at time t_b the refractive index of the medium n_1 is homogeneously changed to n_2. (b) The transmission and reflection of incident EM wave at the temporal boundary t_b along with the direction of respective wave-vectors.

1.6.1 Concept of time-varying media

In a time-varying medium, the refractive index of the medium remains uniform in space and suddenly changes with time. To have a clear idea of such dynamic media, a schematic has been shown in figure 1.6(a) to illustrate the change of the refractive index of the medium from one value to other at a particular time-instant such that,

$$n(t) = \begin{cases} n_1, & \text{for} \quad t < t_b \\ n_2, & \text{for} \quad t > t_b, \end{cases} \tag{1.58}$$

where t_b is the temporal boundary. In such a medium with a temporal boundary, the EM waves no more behaves in a way as it does across a conventional spatial boundary. Let us consider, an EM plane wave of the form,

$$E(\mathbf{r}, t) = E_{in} \exp[i(\mathbf{k} \cdot \mathbf{r} - \omega_{in} t)], \tag{1.59}$$

where E_{in} is the incident wave amplitude, and $k = |\mathbf{k}|$ is the wave vector related to the frequency ω_{in} by the dispersion relation,

$$k = \frac{\omega}{c} n. \tag{1.60}$$

In a time-varying medium as depicted in figure 1.6(a), the transmission and reflection of an incident EM wave E_{in} across a temporal boundary t_b occur according to as shown in figure 1.6(b). For $t < t_b$, the electric field is given by equation (1.59), whereas for $t > t_b$, it is given by [Mendonça and Shukla, 2002],

$$E(\mathbf{r}, t) = E_{tr} \exp[i(\mathbf{k} \cdot \mathbf{r} - \omega_{tr} t)] + E_{re} \exp[i(\mathbf{k} \cdot \mathbf{r} - \omega_{re} t)], \tag{1.61}$$

where E_{tr} and E_{re} represents the transmitted and the reflected wave amplitudes, respectively, and ω_{tr} and ω_{re} are the corresponding frequencies. Important to note that the transmitted wave E_{tr} and the reflected wave E_{re} are on the same side of the temporal boundary, unlike the case of spatial

boundary. This can be explained by the simple argument that going back in time is impossible. Equations (1.59) and (1.61) have to satisfy the dispersion relation given in equation (1.60), which leads to the following expressions:

$$\begin{aligned} \omega_{in} &= \frac{kc}{n_1} \\ |\omega_{re}| &= \omega_{tr} \\ \omega_{tr} &= \omega_{in}\frac{n_1}{n_2}, \end{aligned} \tag{1.62}$$

In this case, the momentum of the light is conserved, however due to the temporal discontinuity, the frequency and in turn the energy of the light is not conserved, i.e. $\omega_{in} \neq \omega_{tr}$, rather is scaled by the ratio of the initial to final refractive index. It is to mention here that the non-conservation of energy leads to an exclusive light dynamics. Also, there is another consequence of the temporal boundary that it introduces a reflected light in space with frequency equal to that of the transmitted light but with opposite momentum. This can be verified from the time continuity conditions for the temporal boundary given by,

$$\mathbf{D}(t < t_b) = \mathbf{D}(t > t_b) \qquad \text{and} \qquad \mathbf{B}(t < t_b) = \mathbf{B}(t > t_b), \tag{1.63}$$

using which one obtains the reflection and the transmission coefficients to be,

$$R = \frac{1}{2}(\delta^2 - 1) \qquad \text{and} \qquad T = \frac{1}{2}(\delta^2 + 1), \tag{1.64}$$

where $\delta = n_1/n_2$. It implies that the absence of reflected wave for $t > t_b$ will not satisfy the continuity condition, and hence it exists with a propagation direction different from the transmitted field. With the understanding of the fundamental characteristics of time-varying media, the dynamics of optical pulses through them can eventually be envisaged. Precisely, pulse frequency shifting without any nonlinear interaction is the prime consequence that may open up new avenues to manipulate light state.

1.6.2 A review on light transmission through time-varying media

In 2002, Mendonça and Shukla demonstrated for the first time the fundamental properties of EM waves across a temporal boundary, namely time-refraction and time-reflection, the two essential features to occur in a non-dispersive dynamic media [Mendonça and Shukla, 2002]. Based on the properties of the temporally varying refractive index, investigations has been performed in two dimensions, one is an adiabatic wavelength conversion process in linear dynamic photonic system [Notomi and Mitsugi, 2006; Tanabe et al., 2009; Khorshidahmad and Kirk, 2010; Upham et al., 2010; Preble et al., 2012; Pang et al., 2021], and on the other hand change in speed of light, photon acceleration, stopping and storing photons [Yanik and Fan, 2004a; Yanik et al., 2004; Povinelli et al., 2005; Gaburro et al., 2006; Kampfrath et al., 2010]. Moreover, there are works that essentially has investigated the behavior of EM waves and optical pulses in dynamically-tuned linear dielectric systems [Yanik and Fan, 2004b; Zurita-Sánchez et al., 2012; Koutserimpas and Fleury, 2018]. At the same time, researchers were investigating on the direct and indirect photonic transitions in silicon based microcavity and waveguides via dynamically tuned refractive index [Dong et al., 2008; Lira et al., 2012]. The domain further gained an alternative direction when Y. Xiao *et. al.* reported a new approach, namely time-transformation method (TTM), to study pulse behavior in a time-dependent refractive index profile [Xiao et al., 2011a]. The TTM method essentially describes a scaling of pulse width and amplitude in a dynamic system with static temporal boundary. By using this method, the various contributions to the reflection and the transmission of EM waves in time-varying medium have been revisited and re-established [Xiao et al., 2014b]. There is a series

of theoretical work by this specific research group where they have described the completeness of their proposed method TTM by implementing it for a nonlinear dispersive medium as well [Xiao et al., 2012, 2013]. Moreover, the behavior of light in dynamically tuned optical resonators have been thoroughly explained by using the modal-expansion theory [Daniel et al., 2011], as well as by using impulse response function of linear systems [Xiao et al., 2011b], both reporting the phenomenon of frequency shifting in the resonator cavity. There are some recent works where the reflection and refraction of optical pulses have been studied in a dispersive medium with moving temporal boundary where the effects of higher order dispersion on pulse spectral behavior have been demonstrated thoroughly [Plansinis et al., 2015, 2016a; Zhang et al., 2021]. Furthermore, nonreciprocal transmission of light has also been investigated recently in some space-time modulated systems [Sounas and Alù, 2017; Taravati, 2018; Guo et al., 2019]. Lately, researchers have been working on waveguides with time-varying refractive index profile that eventually report various novel features of light in such dynamic waveguides [Zhou et al., 2016; Plansinis et al., 2016b; Zeng et al., 2017; Lustig et al., 2018; Sharabi et al., 2021]. However, this dynamic domain of photonics is a growing field of research that requires a large amount of theoretical and experimental observations for its establishment. This thesis partially focuses on the optical pulse behavior crossing the static temporal boundary from counter-propagating direction towards the investigation of nonreciprocal transmission through the dynamic system.

1.7 Scope of the thesis

This thesis has explored the new possibilities towards control and manipulation of states of light through which high power ultrashort pulses can be delivered in the most efficient way targeted for various specialty applications. A thorough literature survey has revealed that there are plenty applications in diverse fields which essentially demands fiber optic based light sources or simply fiber-based delivery of light for their efficient accomplishment. However, the various physical limitations that such ultrashort pulses experience during propagation through fibers consequently has motivated to ideate novel ways of achieving robust light states. Thus, the prime focus of this thesis has been a stable and robust transmission of such high power ultrashort pulses through optical fibers via pulse reshaping technique. It is to mention that the process of pulse reshaping eventually helps to manipulate the various physical conditions in a way to explore the stable light dynamics and robust transmission. For this, a range of specialty optical fibers have been proposed, designed and implemented systematically to address each of the existing challenges hindering their sustainable transmission capacity. The proposed fiber designs have significantly alleviated the distortion of high power ultrashort pulses due to large dispersion and nonlinearity, have unlocked the limitation of small transmission bandwidth of fiber through proper exploitation of bandgap guidance of light, and have achieved a robust state of light that eventually prevents pulse distortion due to back-scattering. The results achieved promises a long distance stable delivery of pulses to a good extent. It is better to emphasize that each fiber design has its own unique way of controlling the adverse influences on light transmission that are readily suitable for the targeted applications. As envisaged from the due course of research, two specific domains may have enough scope for futuristic guided-wave optics.

Enhancement of low-loss transmission bandwidth of the fiber with controlled dispersion and nonlinearity via suitable fiber design process, which are the essential requirements for ultrashort pulse delivery. As it has been observed that the bandwidth of the fiber spans over only a limited spectral range owing to the various loss parameters associated with the fiber. Ultrashort pulses suffer this limited bandwidth effect during the long distance propagation. Moreover, the enhancement in the fiber bandwidth would readily open up new possibilities towards high-capacity data transmission which is now experiencing its saturation level towards the capacity crunch. To find

a breakthrough, novel optical fiber design with ultra-wide bandwidth could possibly be the best technological innovation.

The topology protected light guidance in optical fibers exclusively supports robust and back-reflection free interface states of light. Such innovative topological fibers have huge potential for applications in all-optical network and signal processing, data transmission etc, owing to the robust nature of the topologically protected states of light. It is envisaged that this new mechanism of light guidance would certainly facilitate the development of next-generation guided wave optics forming the basis of beyond 5G or future all-fiber networks.

On the other hand, this thesis has also explored the behavior of ultrashort pulses in time-varying medium which is a growing field of research exhibiting some exclusive states of light suitable for futuristic integrated photonics and signal processing. Some exclusive light dynamics has been explored through such time-varying media which surely have huge scope of advancement in this domain. In this direction, the study of the temporal waveguides and photonic time crystals are already the rapidly evolving areas around the globe. Such time-varying photonic systems can manipulate and control states of light in both the time and frequency domain in a way which are less likely to observe through the conventional space-modulated photonic devices. As the most promising device-level application, linear nonreciprocal photonic devices can be explored through the time-modulation mechanism. In this thesis, a significant research contribution has been made in the aforementioned emerging areas and presented them systematically in context with potential impact and applications.

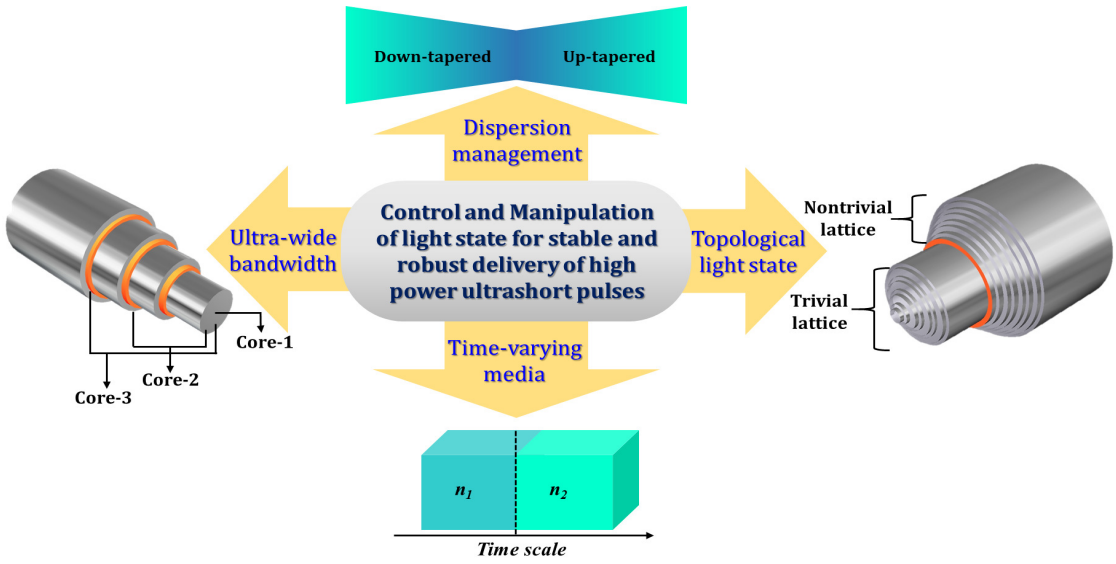

Figure 1.7: The schematic representation of the thesis outline with the study-specific respective physical structures.

1.8 Organization of the thesis

The thesis has been organized as follows. In *Chapter 2*, the theoretical background of the pulse propagation study has been described. For pulse propagation study in fibers, a brief description of nonlinear Schrödinger (NLS) equation along with its modification during pulse reshaping in passive fiber has been given. Moreover, the split-step Fourier method (SSFM) as the numerical technique used for the study of pulse propagation has been provided. For the study of pulse propagation in time-varying media, a novel time-transformation method (TTM) has been described. In

Chapter 3, the formation and stability analysis of high power ultrashort parabolic pulses through a novel input pulse customization process have been presented. A longitudinally tapered fiber with Bragg cross-section exhibiting a decreasing dispersion profile has been designed and optimized for appropriate pulse reshaping technique. Two types of picosecond pulses - one with Gaussian and other with hyperbolic secant form, both combined to a dark optical pulse in their background have been launched to the input of the tapered fiber in the near-infrared wavelength range. A detailed study of the combined pulse evolution through the decreasing dispersion profile has been demonstrated along with a comparative study between the self-similar evolution of background-guided and single pulse forms. In *Chapter 4*, the analysis of stable delivery of high power parabolic pulses in a highly dispersive and highly nonlinear fiber through a novel fiber engineering scheme supporting a rapidly varying longitudinal dispersion profile with a near-zero average normal dispersion has been proposed. Formation and stable propagation of parabolic pulses from high power ultrashort input in both the near and mid-infrared wavelength range have been investigated through the proposed dispersion oscillating fiber. Moreover, effect of higher order dispersion and nonlinearities on the pulse evolution has been studied in-depth. Further, to eliminate the detrimental effect of higher order dispersion on the pulse evolution through the designed fiber, a two-fold fiber engineering scheme comprising a transverse chirping and the longitudinal dispersion variation has been implemented to observe stable pulse delivery. In *Chapter 5*, the issue regarding the enhancement of the low-loss fiber bandwidth for long distance delivery of ultrashort pulses has been addressed with a new fiber design scheme based on the light guidance principle of 1D PBFs. Exhibition of an ultra-wide transmission bandwidth in an all-solid specialty bandgap fiber owing to the number of cores formed effectively due to bandgap mechanism has been discussed in detail. Moreover, both the similariton and soliton formation of femtosecond input pulses through reshaping mechanism and their stable propagation over few kilometers have been presented. In *Chapter 6*, to eliminate the issue of back-reflection and unwanted scattering phenomena in fibers, a topology-protected interface light state have been presented with a specialty topological fiber design based on the band-topology of periodic 1D lattices. A plane wave expansion method has been implemented to characterize the topology of the designed lattices, and the prediction of the interface states has been done from the transmission spectrum of the combined system. Moreover, the modal analysis of the fiber geometry has been carried out using FEM-based numerical analysis. Finally, a detailed study on the pulse propagation and reshaping of pulses through the designed topological fiber have been presented. In *Chapter 7*, the dynamics of ultrashort pulses in a time-varying medium has been thoroughly described. Asymmetric pulse propagation and wavelength shifting in a linear bulk medium with dynamic change of refractive index has been presented. Effect of presence of gain-loss in the system has also been studied. Moreover, a nonreciprocal transmission of light through such linear time-varying system have been theoretically demonstrated. In *Chapter 8*, the entire thesis has been summarized with the future directions, impact statement, and a brief idea about the practical implementation of the proposed photonic devices. Figure 1.7 explicitly depicts the complete outline of this thesis that includes the two prime domains of study related to the stable delivery of high power ultrashort pulses, and the schematics of the guided and the unguided time-varying structures chosen for the respective studies.